J Mater Sci: Mater Med (2013) 24:437–445
DOI 10.1007/s10856-012-4817-x

Zinc-substituted hydroxyapatite: a biomaterial with enhanced bioactivity and antibacterial properties

E. S. Thian · T. Konishi · Y. Kawanobe · P. N. Lim · C. Choong · B. Ho · M. Aizawa

Received: 22 July 2012 / Accepted: 8 November 2012 / Published online: 16 November 2012

Abstract Hydroxyapatite (HA) is a synthetic biomaterial and has been found to promote new bone formation when implanted in a bone defect site. However, its use is often limited due to its slow osteointegration rate and low antibacterial activity, particularly where HA has to be used for long term biomedical applications. This work will describe the synthesis and detailed characterization of zinc-substituted HA (ZnHA) as an alternative biomaterial to HA. ZnHA containing 1.6 wt% Zn was synthesized via a co-precipitation reaction between calcium hydroxide, orthophosphoric acid and zinc nitrate hexahydrate. Single-phase ZnHA particles with a rod-like morphology measuring ~50 nm in length and ~15 nm in width, were obtained and characterized using transmission electron microscopy and X-ray diffraction. The substitution of Zn into HA resulted in a decrease in both the *a*- and *c*-axes of the unit cell parameters, thereby causing the HA crystal structure to alter. In vitro cell culture work showed that ZnHA possessed enhanced bioactivity since an increase in the growth of human adipose-derived mesenchymal stem cells along with the bone cell differentiation markers, were observed. In addition, antibacterial work demonstrated that ZnHA exhibited antimicrobial capability since there was a significant decrease in the number of viable Staphylococcus aureus bacteria after in contact with ZnHA.

E. S. Thian (✉) · P. N. Lim
Department of Mechanical Engineering, National University of Singapore, 9 Engineering Drive 1, Singapore 117 576, Singapore
e-mail: mpetes@nus.edu.sg

E. S. Thian · T. Konishi · Y. Kawanobe · M. Aizawa
Kanagawa Academy of Science and Technology (KAST), 3-2-1 Sakado, Takatsu-ku, Kawasaki, Kanagawa 213-0012, Japan

Y. Kawanobe · M. Aizawa
Department of Applied Chemistry, School of Science and Technology, Meiji University, 1-1-1 Higashimita, Tama-ku, Kawasaki, Kanagawa 214-8571, Japan

C. Choong
School of Materials Science and Engineering, Nanyang Technological University, 50 Nanyang Avenue, Singapore 639 798, Singapore

B. Ho
Department of Mircobiology, National University of Singapore, 10 Kent Ridge Crescent, Singapore 119 260, Singapore

1 Introduction

Calcium phosphate (CaP) family, in particular hydroxyapatite (HA), has been chosen as a synthetic material for biomedical applications due to its bioactivity and osteoconductivity [1]. In addition, HA has a crystallographic and chemical composition approaching to that of the natural bone mineral [2]. This biomaterial has been used in the form of coatings on metallic implants, fillers in polymeric matrices, self-setting bone cements, and even as granules or shaped-structures. However, HA has the disadvantage in which the rate of bone bonding ability is extremely slow [3]. Furthermore, HA does not inhibit bacteria from adhering onto the surface, and this has implications for the bone healing required for patient recovery since infection can lead to the failure of surgical operation [4]. An alternative way to enhance bone fixation and reduce infection is via the incorporation of biological entities such as bone morphogenetic proteins and antibiotics, into HA. However, the beneficial effects of these biological agents have been reported to decline during storage and/or sterilization process [5].

The crystal structure of HA can accommodate substitutions by various beneficial ions easily. As such, there has been an increasing research interest concerning the effects of these ion substitutions. A number of studies introducing silicon-substituted HA have been reported in the literature, and this biomaterial has shown to enhance the rate and quality of bone tissue repair [6–8]. On the other hand, silver-substituted HA has been synthesized by various groups, and demonstrated to reduce bacterial adhesion [9–11]. Though each of these ions has shown to play a significant role in the bone healing process, it is rational to synthesise a HA that exhibits enhanced bioactivity and at the same time, possesses antibacterial property.

Among the various elements that can be substituted, zinc (Zn) seems to be the potential candidate. It is the most abundant trace metallic element found in bone, and an essential metal that plays a crucial role in the biochemistry of bone tissues [12–15]. There has been considerable effort on the synthesis of Zn-substituted HA (ZnHA) [16–20]. The substitution of Zn gave rise to contradictory results on the maximum amount of Zn to be incorporated and the effect on the lattice structure [19, 21]. Sogo et al. [18] reported the formation of α-tricalcium phosphate after heating to 1,050 °C when the incorporated Zn amount exceeded 0.1 wt%. Miyaji et al. [16] found that the substitution limit of Zn to be around 9.4 wt%, beyond which parascholzite phase appeared. Li et al. [22] prepared ZnHA using a hydrothermal method, and the *a* lattice parameter followed a similar reduction–expansion trend at Zn content of 6.4 wt%. On the other hand, the *c* lattice parameter decreased with increased Zn content. Bigi et al. [23] noticed the inhibition of crystallization process with increasing Zn content. Similarly, LeGeros et al. [24] reported the reduction of the degree of crystallinity with zinc substitution. Furthermore, both *a* and *c* lattice parameters was being observed. Ren et al. [21] demonstrated the retention of apatite up to 12.4 wt% of Zn, without any form of heat treatment.

Recently, several works involving Zn-substituted apatite containing low amount of Zn (<1 wt%) have been reported, and shown to exhibit either good bioactivity or antibacterial property [25–28]. Webster et al. [17] found that 1.3 wt% of Zn could be incorporated into HA to enhance osteoblast response. There were also several other studies reporting similar osteoblast response and reduction of osteoclast activity on zinc-substituted tricalcium phosphate (ZnTCP) [18, 28–30]. Ito et al. [28] noted that Zn content of >1.2 wt% in TCP was cytotoxic. Apart from enhanced biological property, ZnHA also possessed antibacterial property. Chung et al. [20] and Stanic et al. [26] observed a reduction of bacterial strains *Escherichia coli* (*E. coli*), *Staphylococcus aureus* (*S. aureus*), *Candida albicans* (*C. albicans*) and Streptococcus mutans (*S. mutans*) on ZnHA. However, no work has actually been directed towards the use of phase-pure ZnHA containing high amount of Zn for potential applications in the orthopaedic and dental fields. This is the first time that phase-pure ZnHA with 1.6 wt% Zn, was synthesized and evaluated using human adipose-derived mesenchymal stem cells (MSCs) and *S. aureus* in this paper.

2 Materials and methods

2.1 Synthesis of ZnHA

Taking into account that a Zn content of >1.2 wt% would result in cytotoxicity [28], and there would be an incomplete substitution of Zn into the HA crystal lattice during synthesis [17, 22], 1.6 wt% of Zn content was selected for this study. ZnHA with a Zn content of 1.6 wt% was synthesized via a wet precipitation method at room temperature using calcium hydroxide [$Ca(OH)_2$] and orthophosphoric acid (H_3PO_4). Zinc nitrate hexahydrate [$Zn(NO_3)_2{\cdot}6H_2O$] was used as the source for Zn, and the amount of reagents required was calculated using the (Ca + Zn)/P molar ratio of 1.67, assuming that Zn would substitute for the Ca site. H_3PO_4 solution was added dropwise into the $Ca(OH)_2$/$Zn(NO_3)_2{\cdot}6H_2O$ mixture solution under continuous stirring condition whilst the pH value as maintained above 10.5 by the addition of aqueous ammonia. Stirring was continued for 18 h after the complete addition of the reactants before the mixture was left to age for 2 weeks. After ageing, centrifugation was performed to remove any excess water from the apatite precipitates. ZnHA was then autoclaved at 124 °C for 2 h.

2.2 Characterisation of ZnHA

The morphology and particle size of ZnHA were examined using a transmission electron microscope (TEM) in bright field mode, operating at an accelerating voltage of 300 kV. Selected area electron diffraction (SAED) was also used to determine the crystal structure. X-ray diffraction (XRD) analysis was performed to identify the phase composition of ZnHA. The diffraction pattern was analysed over a 2θ range of 20–40°, using CuK_α radiation at 40 kV and 40 mA, at a step size of 0.05° and a count time of 10 s. Identification of the phases in ZnHA were compared to the ICDD (JCPDS) standards. Determination of the unit cell parameters (*a* and *c*) of ZnHA was made by Rietveld refinement of the XRD data collected over a 2θ range of 20–80°, with a step size of 0.03° and a dwell time of 20 s. Refinement software was then used based on the structural data for HA of Kay et al. [31]. Infrared spectrum of ZnHA was obtained using a fourier transform infrared (FTIR) spectrophotometer, in the region of 400–4,000 cm^{-1} using a potassium bromide pellets with spectral resolution of 4 cm^{-1}. The amount of Zn being incorporated was determined using an X-ray fluorescence

(XRF) spectroscope. 6 readings were taken, and the mean was calculated. The surface of ZnHA was then analysed by X-ray photoelectron spectroscopy (XPS), with a MgK_{α} radiation (1,253.6 eV) operating at 100 W. A survey spectrum between 0 and 1,100 eV was recorded, and all the binding energies (BEs) were referenced to the C 1 s hydrocarbon peak.

2.3 Biological assessment of ZnHA

2.3.1 Biocompatibility property

ZnHA discs of diameter 12 mm were uni-axially compacted. Cell viability behaviour of ZnHA was evaluated using human adipose-derived MSCs isolated from human lipoaspirate tissue (Invitrogen, StemPro® Human Adipose-Derived Stem Cell Kit, Passage 2). These cells would be thawed and cultured in MesenPRO RS™ medium for a further passage before they were pooled for use in the experiments. ZnHA discs were sterilized by rinsing three times with phosphate buffer saline (PBS) solution, followed by ultraviolet exposure for 30 min. 2×10^4 cells were then seeded on these sterilized ZnHA disc in 1 ml of Dulbecco's modified Eagle medium supplemented with 10 % fetal bone serum and 1 % penicillin–streptomycin, before incubating at 37 °C in a humidified atmosphere of 95 % air and 5 % carbon dioxide. After 10 days of expansion, the growth media would be changed to osteogenic inductive media, which is the growth medium supplemented with 10 mM of β-glycerolphosphate, 100 μM of ascorbic acid and 10^{-8} M of dexamethasone. The growth media was changed every 3 days. HA discs were used as controls, and five replica tests were used for each sample.

2.3.1.1 Cell growth Cell growth over 1, 3 and 5 days was measured using the alamarBlue™ medium. At each time point, cells were cultured in 10 % alamarBlue™ medium for 4 h. The absorbance was then monitored at a wavelength of 570 nm with a reference wavelength of 600 nm.

2.3.1.2 Type I collagen expression Type I collagen (COL) expression was determined by enzyme immunoassay (Metra™ CICP EIA kit). For analysis, culture medium was first diluted with assay buffer at a ratio of 1:3. 100 μl of sample was then added to each well, and incubated at 25 °C for 2 h. Wells were washed three times with 300 μl wash buffer before 100 μl rabbit anti-CICP was added and incubated at 25 °C for 50 min. Wells were again washed three times with wash buffer. Next, 100 μl reconstituted enzyme conjugate was added and incubated at 25 °C for 50 min. A final wash was performed before 100 μl working substrate solution was added and incubated for 30 min. Finally, 50 μl of stop solution was added, and fluorescence was read at 405 nm.

2.3.1.3 Osteocalcin expression Osteocalcin (OCN) level in the culture medium was measured by an enzyme immunoassay (Metra® Osteocalcin ELISA kit). 25 μl of cell medium and 125 μl of anti-osteocalcin antibody were added to each well before incubating at 25 °C for 2 h. Wells were then washed three times with 300 μl wash buffer. Following that, 150 μl reconstituted enzyme conjugate was added, and incubated at 25 °C for 1 h. Wells were again washed three times before 50 μl working substrate solution was added, and incubated at 25 °C for 35 min. Finally, 50 μl of stop solution was added, and fluorescence was read at 405 nm.

2.3.1.4 Immunocytochemistry After 1 day of culture, cells were fixed with 4 % formaldehyde in PBS solution with 1 % sucrose for 15 min, washed with PBS solution and permeabilised at 4 °C for 5 min. They were then incubated with 1 % bovine serum albumin (BSA)/PBS solution at 37 °C for 5 min to block the non-specific binding. FITC-conjugated phalloidin (1:100 in 1 % BSA/PBS) was later added at 37 °C for 1 h. After washing for three times with 0.5 Tween 20/PBS solution for 5 min, TOTO-3 (1:5,000 in Tris/EDTA buffer at pH 8.0) was added at 25 °C for 5 min. The samples were then given a final wash (15 min × 3) before mounting under Vectashield antifade mountant, and viewed on a confocal laser scanning microscope (CLSM).

2.3.1.5 Cell morphology At day 2 and 14, the adherent cells on the samples were fixed with formaldehyde, dehydrated sequentially through a series of ethanol concentrations, and vacuum-dried before viewing under a scanning electron microscope (SEM).

2.3.2 Antibacterial property

Staphylococcus aureus (ATCC 25923) bacteria was used in this study. The discs were immersed in 2 ml of tryptone soya broth containing 4×10^6 cells/ml in a 24-well plate before incubating at 37 °C for 1, 3 and 6 days. After each incubation period, 100 μl of the test solution was retrieved from the 24-well plate, and then subjected to a serial dilution to enumerate the number of surviving colonies. 25 μl of the aliquot of the latter was then added onto a tryptone soya agar with triplicate, and incubated at 37 °C for 1 day for colony formation. The colony formation was examined and counted. The adherent bacteria on the surface of HA and ZnHA discs at day 1 were fixed with formaldehyde, dehydrated sequentially through a series of ethanol concentrations, and vacuum-dried before viewing under SEM. Samples containing only *S. aureus* were used as negative controls.

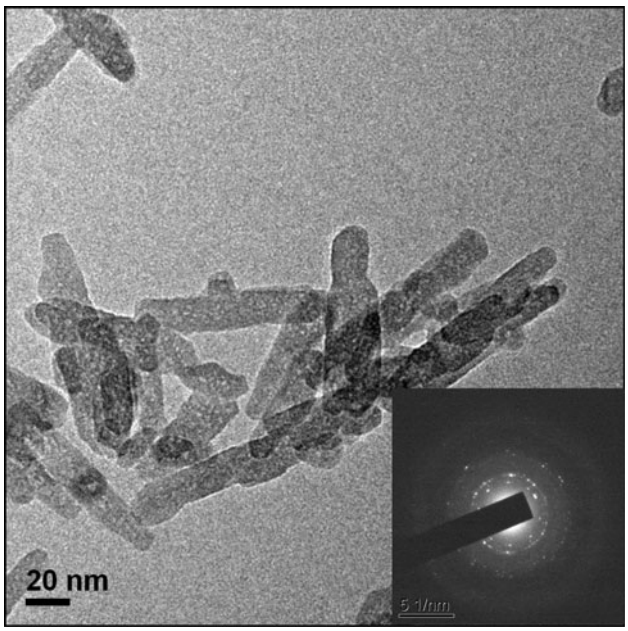

Fig. 1 TEM image and SAED pattern of autoclaved ZnHA

2.4 Statistical analysis

A t test was used to determine whether any significant differences existed between the mean values of the experimental groups. A difference between groups was considered to be significant at $P < 0.05$.

3 Results and discussion

3.1 Physicochemical properties of ZnHA

TEM micrograph of ZnHA particles is shown in Fig. 1. It was observed that ZnHA exhibited a rod-like morphology, measuring ~50 nm long by ~15 nm wide, mimicking that of the natural bone apatite. The SAED image displayed a pattern of continuous rings, indicating that ZnHA has a polycrystalline structure. Despite the incorporation of Zn, the morphology and dimensions of substituted HA remained almost unchanged.

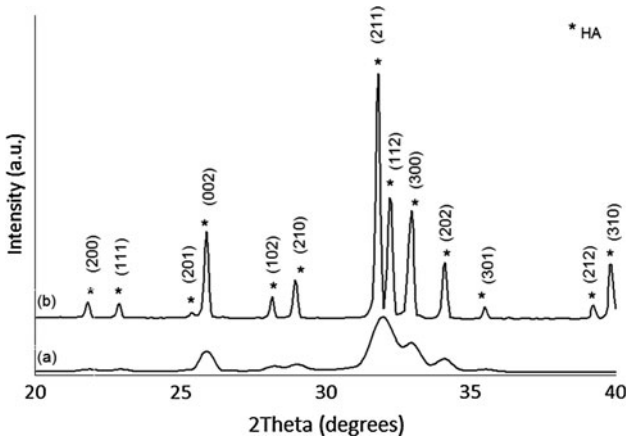

Fig. 2 XRD pattern of autoclaved ZnHA

Table 1 Lattice cell parameters of ZnHA obtained from Rietveld refinement

Sample	Cell parameters[a]	
	a (nm)	c (nm)
HA [21]	0.9418	0.6884
ZnHA	0.9395 (4)	0.6870(4)

[a] Errors are ± standard errors of the mean, with the values in parentheses

Figure 2 shows the XRD pattern of ZnHA. The broad diffraction peaks of ZnHA suggested that this biomaterial was made up of small apatite crystals. Furthermore, the diffraction pattern was not affected by the incorporation of Zn as phase-pure HA was produced. There was no evidence of secondary

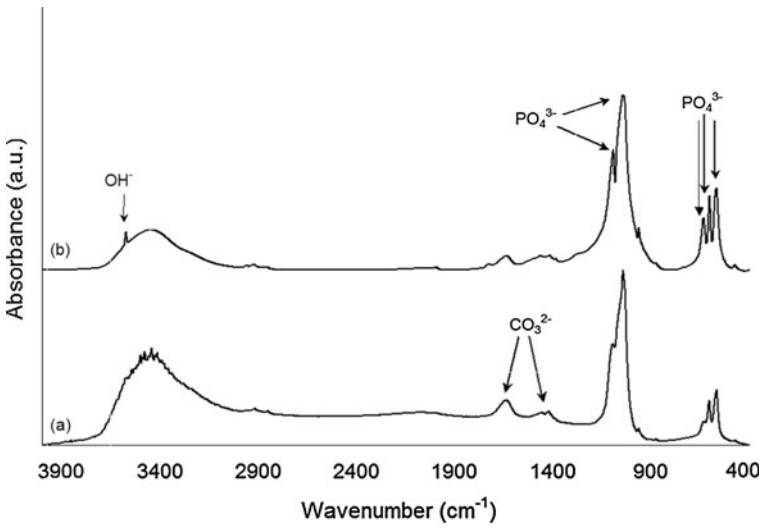

Fig. 3 FTIR spectrum of autoclaved ZnHA

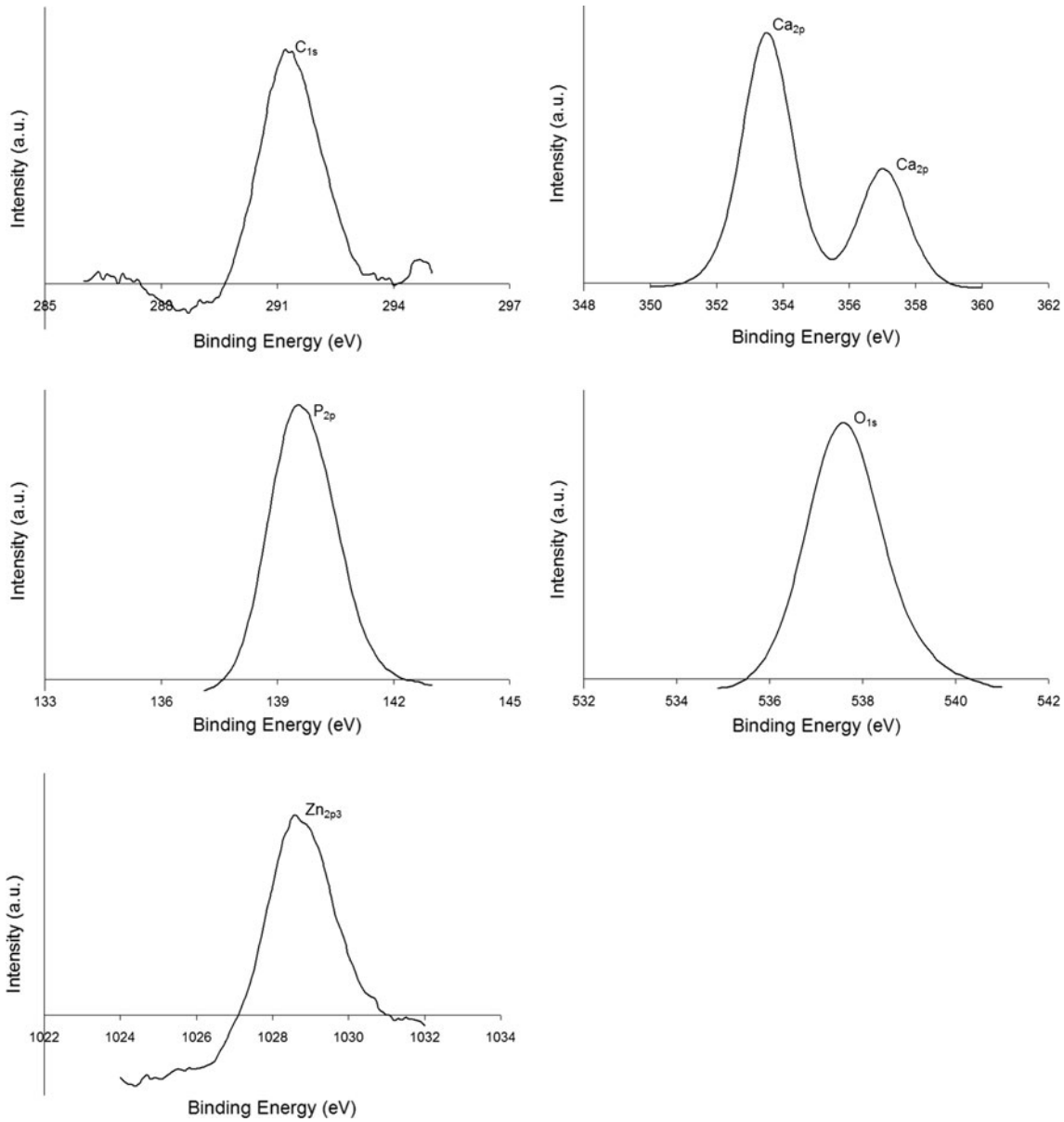

Fig. 4 XPS spectrum of autoclaved ZnHA

undesirable phases such as tricalcium phosphate, tetracalcium phosphate or calcium oxide in the XRD pattern, within the detection limits. Substitution of Zn^{2+} ions into the apatite structure resulted in a change in the lattice cell parameters of ZnHA (Table 1). In this study, both the *a*- and *c*-axes decreased with Zn substitution, following the trend as described by other works [16, 19–22, 32]. The results obtained in the current study are logical since the ionic radius of Zn^{2+} (0.074 nm) is smaller in size than Ca^{2+} (0.099 nm).

The FTIR spectrum of ZnHA is shown in Fig. 3. The absorption bands could be assigned to the phosphate (PO_4^{3-}) vibrations which were characteristics of HA [33]. The v_4 PO_4^{3-} bending bands were located at 562 and 600 cm^{-1} whilst the v_3 PO_4^{3-} stretching bands were centred at 1,037 and 1,089 cm^{-1}. A broad band between 3,300 and 3,700 cm^{-1} was observed in the spectrum which corresponded to the presence of water molecules, thereby obscuring the hydroxyl band at 3,571 cm^{-1}. In addition, v_3 carbonate (CO_3^{2-}) bands were observed at 1,414 and 1,641 cm^{-1}. The substitution of CO_3^{2-} ions could possibly be due to the reaction between carbon dioxide and the precursors during the synthesis process.

The amount of Zn that could be incorporated (1.5 wt%) as measured by XRF was found to be close to the expected value of 1.6 wt%. This phenomenon implied that the substitution of Zn into the Ca site was almost instantaneous during the synthesis process. Figure 4 shows the narrow XPS spectra of ZnHA. It revealed the presence of calcium

(Ca_{2p}) and phosphorus (P_{2p}) peaks. In addition, a peak at binding energy value of ~1,028 eV was observed and assigned to Zn_{2p3}. This result suggested that the synthesized biomaterial was indeed Zn-containing HA, and the values were in agreement with those reported by Wang et al. [25].

From all these physical and chemical analyses, it clearly demonstrated that Zn^{2+} ions were structurally incorporated into the HA crystal structure by replacing the Ca^{2+} ions, rather than existing as a second phase with HA. Thus, the chemical formula in which substitution of Zn into the HA can be represented as follows:

$$Ca_{10-x}Zn_x(PO_4)_6(OH)_2$$

3.2 Biological properties of ZnHA

There were no studies in the literature reporting on the investigation of ZnHA towards cellular proliferation and differentiation. Webster et al. [17] only reported that the incorporation of Zn into HA enhanced osteoblast adhesion and differentiation, with increased levels of alkaline phosphatase activity and deposition of calcium-containing minerals. As such, a detailed in vitro study of ZnHA will be discussed in this work. alamarBlue™ assay indicated that the growth activity of MSCs on both HA and ZnHA increased significantly with culturing time (Fig. 5). However, cells tended to multiply significantly (t test, $P < 0.05$) on ZnHA as compared to HA at day 3 and 5, demonstrating that ZnHA was an excellent bioactive material.

The level of protein expression on HA and ZnHA was also determined. An increase in COL expression was noted from day 14 to 28, and day 14 to 21 for HA and ZnHA, respectively. A significant amount of COL (t test, $P < 0.05$) was being produced on ZnHA as compared to HA, at day 14 and 21 (Fig. 6a). In addition, OCN was detected on HA and ZnHA from day 14 onwards, and

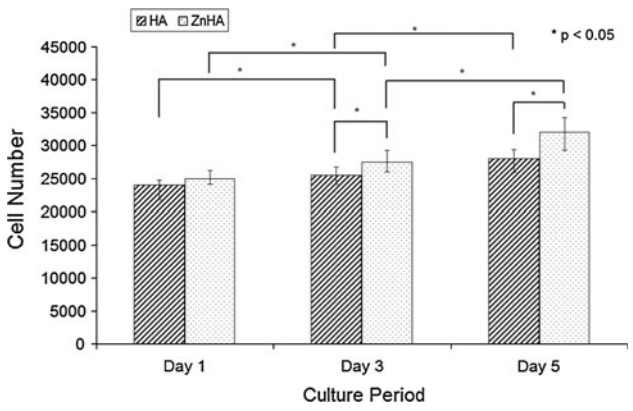

Fig. 5 Growth of MSCs on HA and ZnHA at various time points

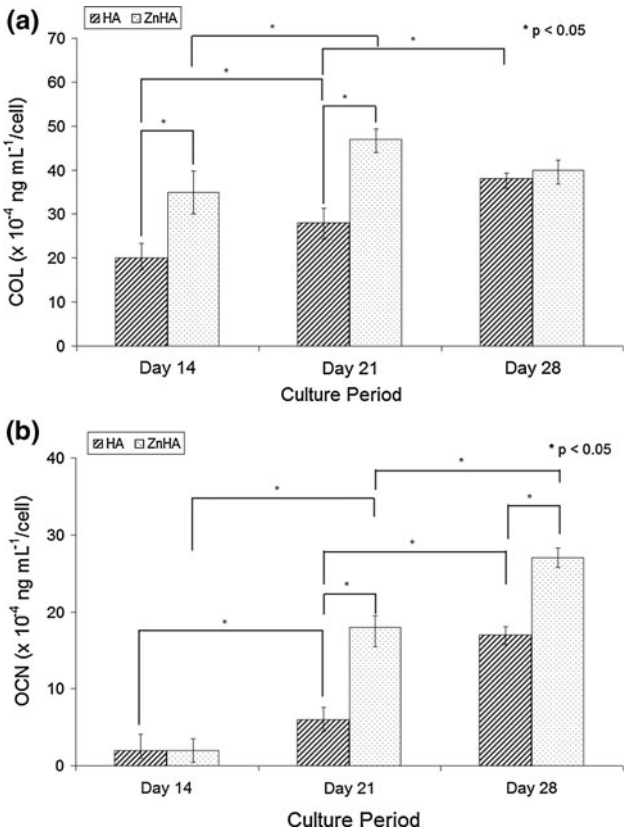

Fig. 6 Quantitative measurement of protein expression on HA and ZnHA

increased significantly (t test, $P < 0.05$) with culturing time (Fig. 6b). However, a significant amount of OCN protein was observed at day 21 and 28 for ZnHA when comparing both samples.

Fluorescent microscopy revealed that cells were attaching and stretching (red in colour) well on ZnHA at day 1 (Fig. 7). This phenomenon was supported by the SEM images, indicating numerous filopodia projecting from the cell edges for ZnHA at day 2 (Fig. 8a). No significant difference could be observed when comparing to HA. After 14 days of culturing, biomineralisation seemed to occur on ZnHA (Fig. 8b) since CaP mineral nodules could be observed. However, this was not the case for HA.

These findings demonstrated that the substitution of Zn in minute amount (1.6 wt%) into HA, plays a significant role in promoting cell growth and differentiation. Nevertheless, the mechanism in which how Zn affects the biological response still requires further investigation.

From the log reduction assay results, it was found that there was a general increase in the number of *S. aureus* from the starting population of 4×10^6 CFU/ml for both samples within the first day, with a 2-log and 1-log increment for HA and ZnHA, respectively (Fig. 9).

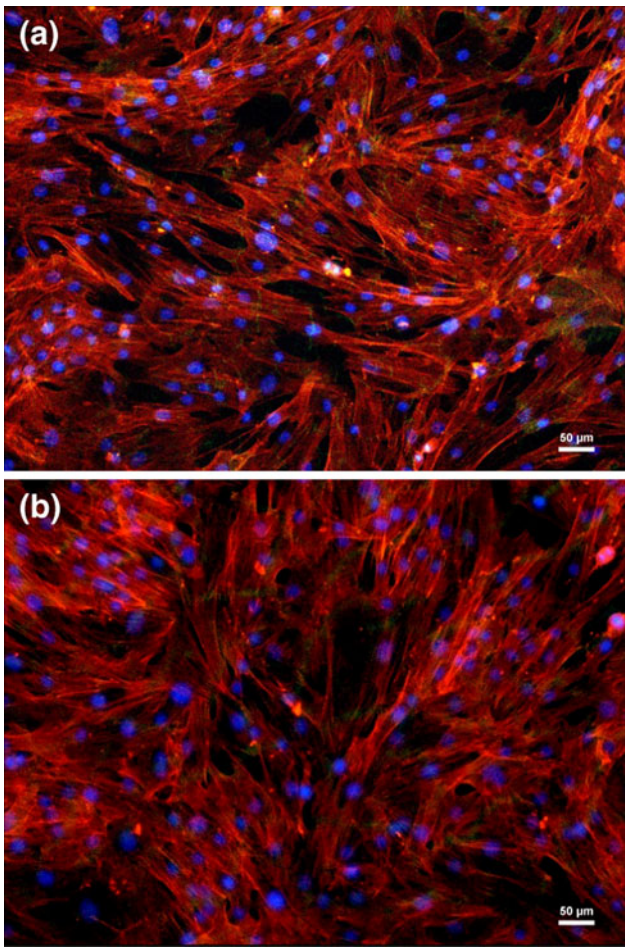

Fig. 7 Fluorescent microscopy images of MSCs cultured at day 1 on **a** HA, and **b** ZnHA. Stress fibers (*stained red*), and cell nuclei (*stained blue*) (Color figure online)

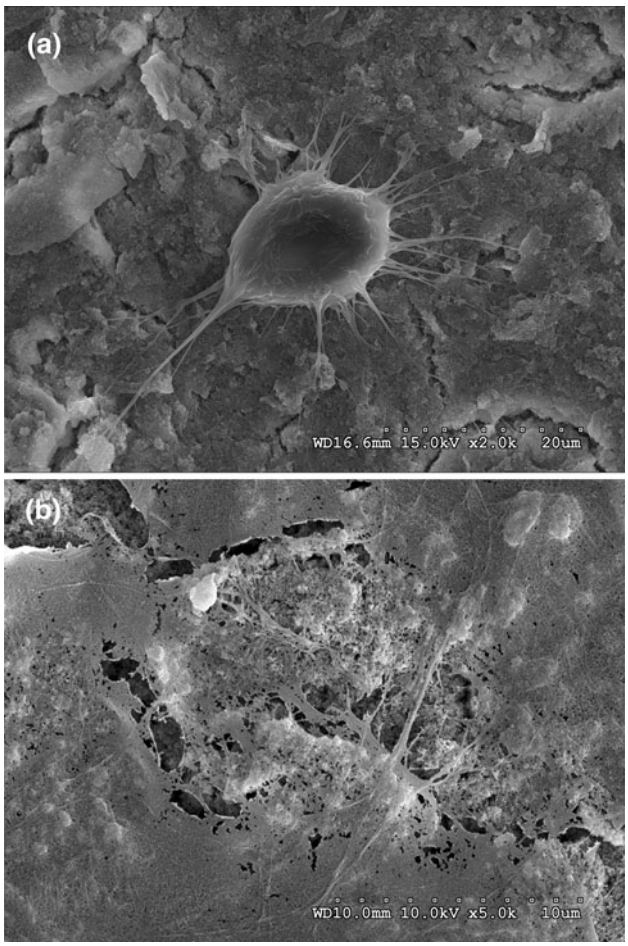

Fig. 8 SEM images of MSCs cultured on ZnHA. **a** Numerous filopodia projecting from cell edges at day 2; and **b** Evidence of biomineralisation occurring at day 14

However at day 3, there was a 1-log and 2-log reduction in the number of bacteria observed in HA and ZnHA, respectively. By day 6, there was a further 6-log reduction in the numbers of bacteria for ZnHA, but the numbers of bacteria seemed to remain unchanged for HA. For the negative control, the numbers of bacteria tend to grow with culturing time until it reached a plateau. In general, viable *S. aureus* colonies could still be observed for HA, but no viable colonies could be seen after day 6 for ZnHA. Chung et al. [20] observed the suppression of the growth of *S. mutans* colonies surrounding ZnHA-coated sample whereas Stanic et al. [26] demonstrated no zone of diffusion in ZnHA samples, but viable cell reduction for *E. coli*, *C. albinos*, *S. aureus*. Recently, Swetha et al. [34] observed a reduction of the growth of *S. aureus* when in contact with ZnHA up to 6 days. All these studies demonstrated similar phenomenon such that ZnHA showed viable cell reduction of *E. coli*, *C. albinos*, *S. aureus* and *S. mutans* which support the current findings.

At day 1, a confluent bacterial layer was found on the surface of HA (Fig. 10a) whilst fewer numbers of bacteria were seen attaching on the surface of ZnHA (Fig. 10b). The SEM observation seemed to correspond well with the results obtained from the log reduction assay, suggesting that ZnHA was capable of inhibiting bacterial growth.

Based on this work, one could deduce that ZnHA possessed antimicrobial property, inhibiting bacterial growth over time. Du et al. [35] reported that chitosan nanoparticles loaded with copper ions interacted with the membranes of *E. coli*, causing structural change and hence, cell death. On the other hand, Nan et al. [36] reported that membranes of *E. coli* were seriously damaged after in contact with the stainless steel containing copper ions, thereby causing nutrients, proteins and other essential components of the cytoplasm within the bacteria to 'leak out' and hence, resulting cell death. It was hypothesized that in this study, Zn^{2+} ions would behave similarly to Cu^{2+} ions to form strong bonds with the membrane proteins of *S. aureus* bacteria, causing structural changes to the

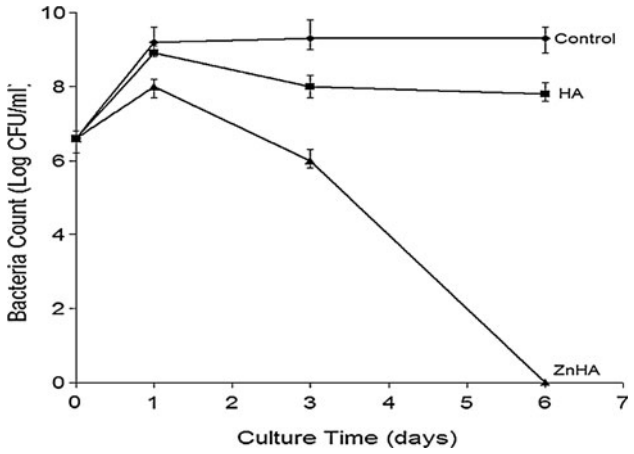

Fig. 9 Log reduction against *S. aureus* for various samples

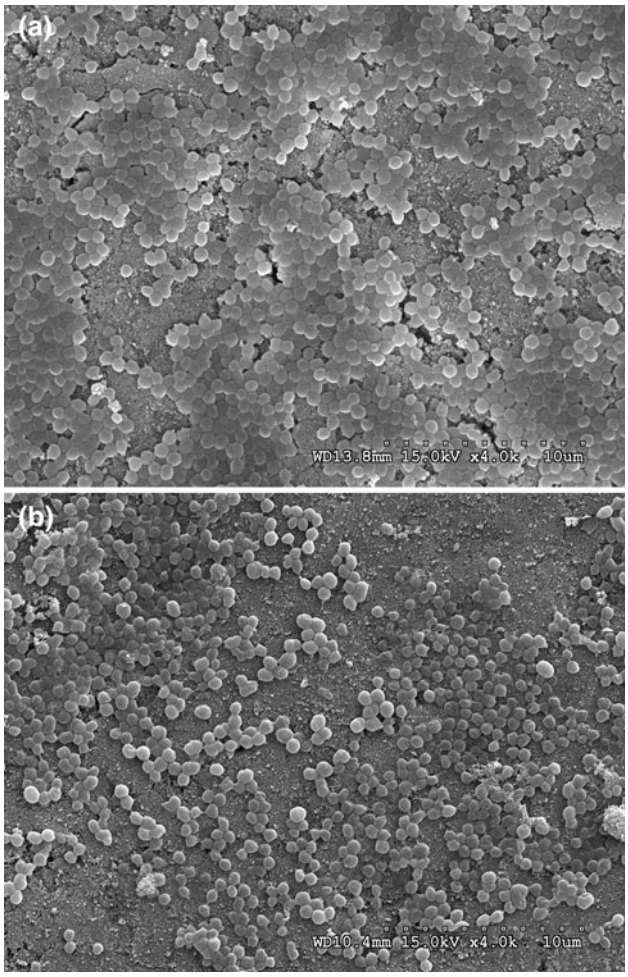

Fig. 10 SEM images of viable *S. aureus* attaching on **a** HA, and **b** ZnHA at day 1

membranes, thereby affecting proper nutrient/protein transport through the nuclei via the membranes and hence, contributing to cell death [26]. Although there have been several works in the literature describing the mechanism of antimicrobial activity of various materials, the actual mechanism in which how Zn interacts with the bacteria's membrane and thereby, activates antimicrobial property, should be investigated further.

4 Conclusions

ZnHA containing 1.6 wt% Zn was synthesized via a co-precipitation reaction at room temperature. Rod-like, single-phase ZnHA particles measuring ~50 nm in length and ~15 nm in width, were obtained. The unit cell parameters (both *a*- and *c*-axes) decreased with the substitution of Zn. ZnHA retained its typical HA characteristics despite the incorporation of Zn. The in vitro cellular response indicated an increase in the growth of human adipose-derived MSCs on ZnHA, along with an enhancement in the bone cell differentiation markers. From the antibacterial study, it was demonstrated that viable *S. aureus* bacteria reduction could be observed on ZnHA. All these findings confirmed the enhanced bioactivity and antimicrobial property of ZnHA as an alternative biomaterial to phase-pure HA.

Acknowledgments This research was supported by Hitachi Scholarship Foundation (Japan) under Research Fellowship HSF-R126.

References

1. De Groot K, Wolke J. Calcium phosphate coatings for medical implants. Proc Instn Mech Eng. 1998;212H:137–47.
2. Oonishi H. Orthopaedic applications of hydroxyapatite. Biomaterials. 1991;12:171–8.
3. Oonishi H, Hench LL, Wilson J, Sugihara F, Tsuji E, Kushitani S, Iwaki H. Comparative bone growth behavior in granules of bioceramic materials of various sizes. J Biomed Mater Res. 1999;44:31–43.
4. Darouiche RO. Treatment of infections associated with surgical implants. Infect Dis Clin Pract. 2004;12:258–9.
5. Yazdi M, Bernick S, Paule W, Nimni M. Postmortem degradation of demineralised bone matrix osteoinductive potential: effect of time and storage temperature. Clin Orthop Relat Res. 1991;262:281–5.
6. Thian ES, Huang J, Best SM, Barber ZH, Brooks RA, Rushton N, Bonfield W. The response of osteoblasts to nanocrystalline silicon-substituted hydroxyapatite thin films. Biomaterials. 2006; 27:2692–8.
7. Porter AE, Patel N, Skepper JN, Best SM, Bonfield W. Effect of sintered silicate-substituted hydroxyapatite on remodelling processes at the bone-implant interface. Biomaterials. 2004;25: 3303–14.
8. Patel N, Best SM, Bonfield W, Gibson IR, Hing KA, Damien E, Revell PA. A comparative study on the in vivo behavior of hydroxyapatite and silicon substituted hydroxyapatite granules. J Mater Sci Mater Med. 2002;13:1199–206.
9. Chen Y, Zheng X, Xie Y, Ji H, Ding C, Li H, Dai K. Silver release from silver-containing hydroxyapatite coatings. Surf Coat Tech. 2010;205:1892–6.

10. Rameshbabu N, Kumar TSS, Prabhakar TG, Sastry VS, Murty KVGK, Rao KP. Antibacterial nanosized silver substituted hydroxyapatite: synthesis and characterization. J Biomed Mater Res. 2007;80A:581–91.
11. Kim TN, Feng QL, Kim JO, Wu J, Wang H, Chen GC, Cui FZ. Antimicrobial effects of metal ions (Ag+, Cu2+, Zn2+) in hydroxyapatite. J Mater Sci Mater Med. 1998;9:129–34.
12. Ito A, Otsuka M, Kawamura H, Ikeuchi M, Ohgushi H, Sogo Y, Ichinose N. Zinc-containing tricalcium phosphate and related materials for promoting bone formation. Curr Appl Phys. 2005;5:402–6.
13. Rossi L, Migliaccio S, Corsi A, Marzia M, Bianco P, Teti A, Gambelli L, Cianfarani S, Paoletti F, Branca F. Reduced growth plate activity and inanition. J Nutr. 2001;131:1142–6.
14. Moonga BS, Dempster DW. Zinc is a potent inhibitor of osteoclastic bone resorption in vitro. J Bone Min Res. 1995;10:453–7.
15. Yamaguchi M, Oishi H, Suketa Y. Stimulatory effect of zinc on bone formation in tissue culture. Biochem Pharma. 1987;36: 4007–12.
16. Miyaji F, Kono Y, Suyama Y. Formation and structure of zinc-substituted calcium hydroxyapatite. Mater Res Bull. 2005;40:209–20.
17. Webster TJ, Massa-Schlueter EA, Smith JL, Slamovich EB. Osteoblast response to hydroxyapatite doped with divalent and trivalent cations. Biomaterials. 2004;25:2111–21.
18. Sogo Y, Ito A, Fukasawa K, Sakurai T, Ichinose N. Zinc containing hydroxyapatite ceramics to promote osteoblastic cell activity. Mater Sci Tech. 2004;20:1079–83.
19. Ergun C, Webster TJ, Bizios R, Doremus RH. Hydroxylapatite with substituted magnesium, zinc, cadmium, and yttrium. I. Structure and microstructure. J Biomed Mater Res. 2002;59:305–11.
20. Chung R, Hsieh M, Huang C, Perng L, Wen H, Chin T. Antimicrobial effect and human gingival biocompatibility of hydroxyapatite sol-gel coatings. J Biomed Mater Res. 2006;76B:169–78.
21. Ren F, Xin R, Ge X, Leng Y. Characterization and structural analysis of zinc-substituted hydroxyapatites. Acta Biomater. 2009;5:3141–9.
22. Li MO, Xiao X, Liu R, Chen C, Huang L. Structural characterization of zinc-substituted hydroxyapatite prepared by hydrothermal method. J Mater Sci Mater Med. 2008;19:797–803.
23. Bigi A, Foresti E, Gandolfi M, Gazzano M, Roveri N. Inhibiting effect of zinc on hydroxyapatite crystallisation. J Inorg Biochem. 1995;58:49–58.
24. LeGeros R, LeGeros J. Dense hydroxyapatite. In: Hench LL, Wilson J, editors. An introduction to bioceramics. Singapore: World Scientific; 1993. p. 139–80.
25. Wang X, Ito A, Sogo Y, Li X, Oyane A. Zinc-containing apatite layers on external fixation rods promoting cell activity. Acta Biomater. 2010;6:962–8.
26. Stanić V, Dimitrijević S, Antić-Stanković J, Mitrić M, Jokić B, Plećaš I, Raičević S. Synthesis, characterization and antimicrobial activity of copper and zinc-doped hydroxyapatite nanopowders. Appl Surf Sci. 2010;256:6083–9.
27. Sogo Y, Sakurai T, Onuma K, Ito A. The most appropriate (Ca + Zn)/P molar ratio to minimize the zinc content of ZnTCP/HAP ceramic used in the promotion of bone formation. J Biomed Mater Res. 2002;62:457–63.
28. Ito A, Ojima K, Naito H, Ichinose N, Tateishi T. Preparation, solubility, and cytocompatibility of zinc-releasing calcium phosphate ceramics. J Biomed Mater Res. 2000;50:178–83.
29. Yamada Y, Ito A, Kojima H, Sakane M, Miyakawa S, Uemura T, LeGeros RZ. Inhibitory effect of Zn_2+ in zinc-containing β-tricalcium phosphate on resorbing activity of mature osteoclasts. J Biomed Mater Res. 2008;84A:344–52.
30. Kawamura H, Ito A, Miyakawa S, Layrolle P, Ojima K, Ichinose N, Tateishi T. Stimulatory effect of zinc-releasing calcium phosphate implant on bone formation in rabbit femoral. J Biomed Mater Res. 2000;50:184–90.
31. Kay MI, Young RA, Posner AS. Crystal structure of hydroxyapatite. Nature. 1964;204:1050–2.
32. Hayakawa S, Ando K, Tsuru K, Osaka A, Fujii E, Kawabata K, Bonhomme C, Babonneau F. Structural characterization and protein adsorption property of hydroxyapatite particles modified with zinc ions. J Am Ceram Soc. 2007;90:565–9.
33. Rehman I, Bonfield W. Characterization of hydroxyapatite and carbonated apatite by photo acoustic FTIR spectroscopy. J Mater Sci Mater Med. 1997;8:1–4.
34. Swetha M, Sahithi K, Moorthi A, Saranya N, Saravanan S, Ramasamy K, Srinivasan N, Selvamurugan N. Synthesis, characterization, and antimicrobial activity of nano-hydroxyapatite-zinc for bone tissue engineering applications. J Nanosci Nanotech. 2012;12:167–72.
35. Du WL, Xu YL, Xu ZR, Fan CL. Preparation, characterization and antibacterial properties against E. coli K 88 of chitosan nanoparticle loaded copper ions. Nanotechnology. 2008;19:085707.
36. Nan L, Liu Y, Lü M, Yang K. Study on antibacterial mechanism of copper-bearing austenitic antibacterial stainless steel by atomic force microscopy. J Mater Sci Mater Med. 2008;19:3057–62.